Appl Nanosci (2015) 5:105–114
DOI 10.1007/s13204-014-0297-2

ORIGINAL ARTICLE

Structural, magnetic and electrical properties of the lithium ferrite obtained by ball milling and heat treatment

S. A. Mazen · N. I. Abu-Elsaad

Received: 30 November 2013 / Accepted: 28 January 2014 / Published online: 27 February 2014

Abstract The physical properties of ferrites are very sensitive to microstructure, which in turn critically depends on the manufacturing process. Lithium ferrite is synthesized by milling process. The powder was annealed at four different temperatures 600, 800, 1,000 and 1,200 °C. The powder annealed at 600 °C has the spinel structure with some of α-Fe_2O_3, while the powders annealed at ≥800 °C formed in single-phase cubic spinel structure. Particle size of lithium ferrite is in the range of 26–70 nm, and is dependent on the annealing temperature. The saturation magnetization increased from 22 to 85 emu/g and the coercivity decreases from 124 to 4 Oe with increase in the annealing temperature. The dielectric constant (ε'), dielectric loss (tan δ) and ac conductivity (σ_{ac}) were measured at room temperature as a function of frequency. The results of dielectric properties were explained in terms of Koops phenomenological theory.

Keywords Li-ferrite · Milling · Annealing temperature · Magnetization · Conductivity

Introduction

Recently, the material science research is focused on the invention of new materials with the enhanced properties and novel synthesis techniques to cope up with the increased technological demand. Nanocrystalline materials are the centre of the attention due to their tremendous applications and interesting properties (Hashim et al. 2012). New physical properties and new technologies both in sample preparation and device fabrication evoke on account of the development of nanoscience (Tzeng Lue 2007). Lithium ferrite ($Li_{0.5}Fe_{2.5}O_4$) is one of the most versatile magnetic materials for common use, having many applications in both low- and high-frequency devices. It plays a useful role in many technological applications such as microwave devices, power transformers in electronics, rod antennas, read/write heads for high-speed digital tapes due to its high resistivity, high Curie temperature and chemical stability (Bellad et al. 1999; Bahgat et al. 2007).

The method of preparation, chemical composition, annealing temperature and duration, grain size, and doping additives play an important role for tailoring properties of spinel ferrites for various applications. Recently, $Li_{0.5}Fe_{2.5}O_4$ nanoparticles have been developed via several techniques like sol–gel auto-ignition (Shirsath et al. 2011), oxalate precursor (Hessien 2008), Flash combustion and Citrate precursor (Verma et al. 2009). However, no reports have been found so far in the literature describing the preparation of nanocrystalline lithium ferrite by milling process. Therefore, in the present research, the milling process has been used to prepare lithium ferrite powders, as in this simple, low-cost and environmental friendly method. Further, the structural, magnetic and electrical properties have been studied as a function of annealing temperature.

Experimental

Sample preparation

Lithium ferrite ($Li_{0.5}Fe_{2.5}O_4$) was produced by high-energy ball milling. The initial materials were Li_2CO_3 (Sigma-Aldrich, 99 wt%) and α-Fe_2O_3 (Sigma-Aldrich, 99 wt%).

S. A. Mazen (✉) · N. I. Abu-Elsaad
Magnetic Semiconductor Laboratory, Physics Department, Faculty of Science, Zagazig University, Zagazig, Egypt
e-mail: dr.saidmazen@gmail.com

The powders were first hand ground in an agate mortar and then milled in a planetary ball mill. High-energy ball milling of the homogeneous powder mixture was carried out with a planetary ball mill (Model Fritsch Pulverisatte-6). In the planetary ball mill, a rotating disk carries vials that rotate in opposite direction every 10 min. The rotation of speed was 150 rpm under air atmosphere for 15 h. Then the powder was pressed in a disk-shaped form of 13-mm diameter, and 3- to 5-mm thickness. Finally, the synthesized samples were heat treated at different temperatures at 600, 800, 1,000 and 1,200 °C for 2 h in a programmable furnace with a heating rate of 5°/min and a cooling rate of 2°/min.

Characterization of samples

Phase analysis of lithium ferrite samples prepared by the two methods was investigated by X-ray diffractometer, XRD, employing Cu K_α radiation ($\lambda = 1.5405$ Å) (type *PHILIPS X'Pert* Diffractometer). The XRD patterns were recorded at room temperature in 2θ range of 10°–90°. The particle size of the samples was calculated using the Sherrer's relation (Cullity 1959):

$$t = \frac{0.9\lambda}{\beta \cos\theta} \tag{1}$$

where t is the particle diameter, λ is the wavelength of X-ray radiation, θ is Bragg's angle, β is the full width at half maximum.

The particle morphology was examined using a transmission electron microscope (TEM) model, Jeol "**JEM-1230**".

The X-ray density, 'd_x' was computed from the values of the lattice parameter using the formula (Cullity 1959):

$$d_x = \frac{8M}{Na^3} \tag{2}$$

where 8 represents the number of molecules per unit cell of spinel lattice. M is molecular weight, N is Avogadro's number and $(V = a^3)$ is the volume of the cubic unit cell.

The experimental bulk density was calculated using the relation:

$$d = \frac{m}{V} = \frac{m}{\pi r^2 h} \tag{3}$$

where m, V, r and h are the mass, volume, radius and the thickness of the sample, respectively.

The percentage porosity (P %) of each sample was calculated using the formula (Standley 1972):

$$P\% = 100\left(1 - \frac{d}{d_x}\right). \tag{4}$$

For recording IR spectra, powders were mixed with KBr in the ratio 1:100—by weight—to ensure uniform dispersion in the KBr pellet. The IR spectra patterns were recorded at 300 K on Perkin–Elmer IR spectrometer in the wave number range 200–1,500 cm^{-1}.

Magnetic measurements

A vibrating sample magnetometer (VSM) was used to investigate the magnetic properties of the samples at room temperature. The maximum applied external field was 7 kOe. By applying this technique, parameters like specific saturation magnetization (M_s) and coercive force (H_c) can be deduced.

Electrical measurements

The prepared samples were coated on adjacent faces with silver paste, thereby forming parallel-plate capacitor geometry. The dc and ac electrical conductivity measurements were carried out using the two-probes method over a wide range of elevated temperatures from 300 K up to well below the annealing temperature using Fluke PM 6306 LCR Hi tester. The ac electrical conductivity was measured in the range of frequencies from 10^2 to 10^6 Hz.

The ac conductivity measurements were carried out using the complex impedance technique. The dielectric constant (ε') and then dielectric loss (ε'') were calculated from ac conductivity ($\tilde{\sigma}$) and the dielectric loss tangent (tan δ) using the formulae (Smit and Wijn 1959)

$$\varepsilon'' = 1.8 \times 10^{10} \frac{\tilde{\sigma}}{f} \tag{5}$$

$$\varepsilon' = \frac{\varepsilon''}{\tan\delta} \tag{6}$$

where f is the frequency of the applied field.

Results and discussion

X-ray analysis

Figure 1 illustrates the XRD patterns for lithium ferrite as prepared and annealed at different temperatures (600, 800, 1,000 and 1,200 °C). It is evident that the powder as prepared is not in a single phase. At the annealing temperature 600 °C, the pattern is composed of spinel-type $Li_{0.5}Fe_{2.5}O_4$ with some of α-Fe_2O_3. For the annealing temperature above 600 °C, the lithium ferrite is formed in spinel structure confirming all the peaks in the pattern matching well with JCPDS card. No secondary phases are detected in the XRD patterns of the samples. The peaks can be indexed to (220), (311), (400), (421), (422), (511) and (440) planes of a cubic unit cell, which are corresponding to cubic spinel structure.

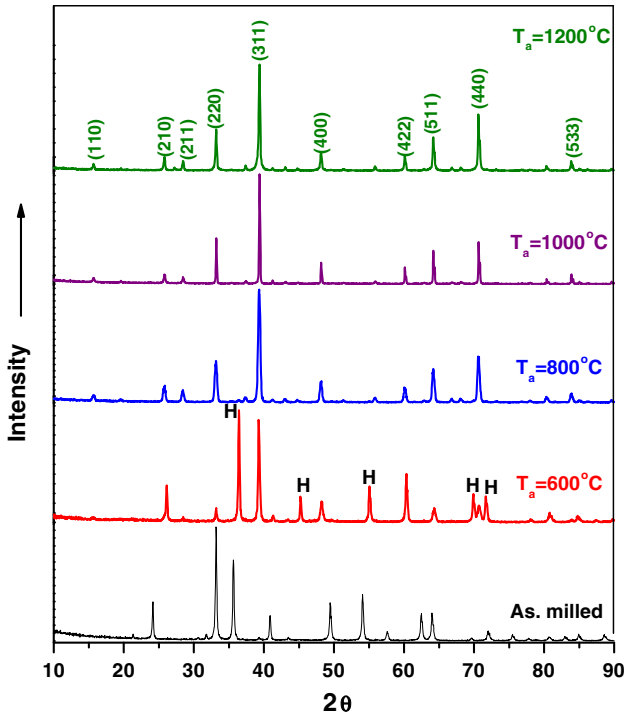

Fig. 1 XRD patterns of $Li_{0.5}Fe_{2.5}O_4$ particles

Table 1 The calculated values of the lattice parameter (*a*) and the particle size (t)

Annealing temperature (°C)	*a* (nm)	*t* (nm)	
		XRD	TEM
600	0.829	26.49	–
800	0.832	27.41	35–45
1,000	0.833	69.58	–
1,200	0.834	–	–

It is observed that as the annealing temperature increases, the width of the central maxima (311) decreases. This is due to the particle size increase with increase in the annealing temperature (T_a). The particle size (*t*) of the annealed samples at 600, 800 and 1,000 °C was obtained from the full width at half maxima (FWHM) of the (311) peak using the well-known Sherrer's equation (Cullity 1959). The particle size for the annealed powder at 1,200 °C was not calculated because of limitations of Debye Sherrer's relation (Verma et al. 2009). The values of particle size are presented in Table 1. The particle size of all the samples is found in the range between 26 and 70 nm. The values of the particle size are observed to be increased with increasing the annealing temperature. This may be due to the enhancement of the crystallinity with temperature.

The TEM image of $Li_{0.5}Fe_{2.5}O_4$ annealed at 800 °C is shown in Fig. 2, as an example, the powders reveal a range of size from 35 to 45 nm. It is seen from the figure that

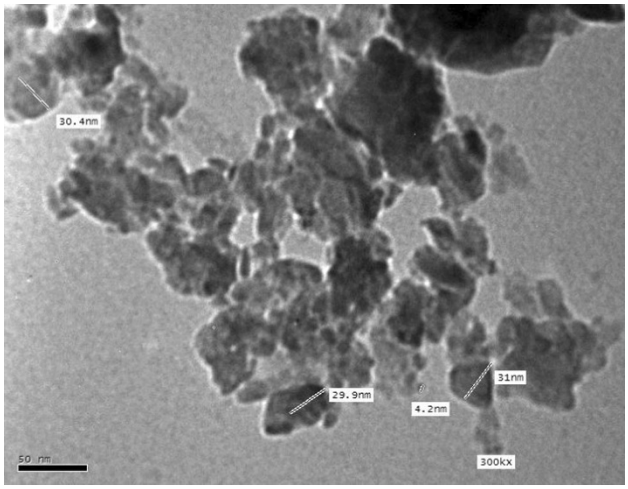

Fig. 2 TEM image for the sample annealed at 800 °C

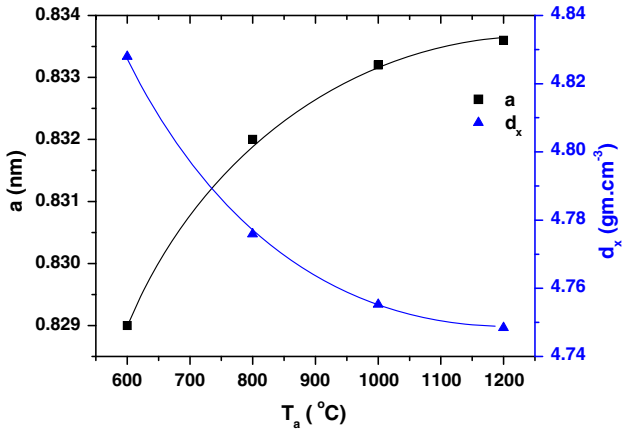

Fig. 3 The variation of lattice parameter '*a*' and X-ray density with annealing temperature

most of the particles appear as spherical in shape; however, some moderately agglomerated particles as well as separated particles are present in the image. Agglomeration of the particles can be attributed to the interaction between magnetic nanoparticles. The obtained particle size is bit higher than that estimated by Scherrer formula from XRD data.

The experimental lattice parameter 'a' was calculated from XRD data. It was found to be in the range of 0.829–0.834 nm, which is within the range of that mentioned in JCPDS card (0.833 nm for lithium ferrite). The variation of the lattice parameter with annealing temperature is clearly shown in Fig. 3. It is observed that the lattice constant increases by increasing the annealing temperature. This behaviour may be attributed to the expansion of the whole lattice by increasing the annealing temperature. The uniform increase in the lattice constant with the annealing temperature indicates that the lattice expands without disturbing the symmetry of lattice.

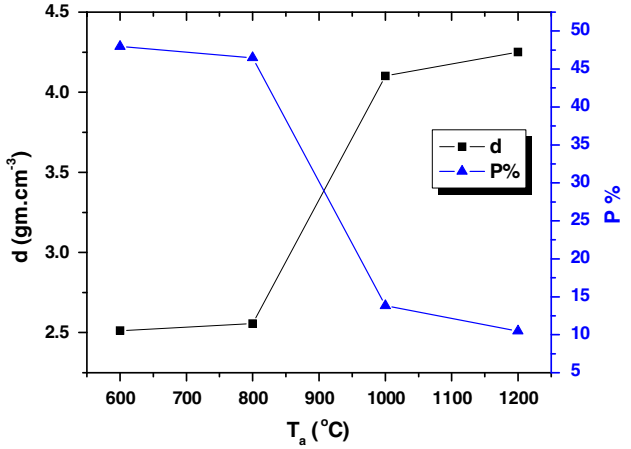

Fig. 4 The effect of annealing temperature on bulk density and percentage porosity

The variation of X-ray density (d_x) with the annealing temperature is displayed in Fig. 4. It is observed that the X-ray density decreases with increasing the annealing temperature T_a. The decrease in X-ray density may be related to the lattice constant, where the lattice constant increases with increasing the annealing temperature. Because the lattice constant is inversely proportional to the annealing temperature and the molecular weight is constant for each sample, this leads to the observed decrease in the X-ray density.

The variation of both bulk density '*d*' and percentage porosity (*P* %) as a function of annealing temperature is shown in Fig. 4. It is clear from the figure that the density of the samples increases and the porosity decreases with increasing the annealing temperature. This is an evidence of accelerated densification during the annealing process which leads to a reduction of the porosity and enhancement of the crystallinity of the samples (Akther Hossain et al. 2007).

IR absorption spectra analysis

According to Waldron (1955), the ferrites can be considered continuously bonded crystal, according to which, the atoms are bonded to all nearest neighbours by equivalent forces (ionic, covalent or Van der Waals). In ferrites, the metals ions are situated in two different sublattices designated tetrahedral (A-site) and octahedral (B-site) according to the geometrical configuration of the oxygen nearest neighbours. Waldron (1955) and Hafner (1961) have attributed the band around 600 cm^{-1} to stretching vibrations of the tetrahedral groups (υ_1^*) and that around 400 cm^{-1} to the octahedral groups (υ_2^*).

The IR spectra for the powder in the main form of $Li_{0.5}Fe_{2.5}O_4$ as prepared and annealed at different temperatures (600, 800, 1,000 and 1,200 °C) were recorded in the range of 200–1,500 cm^{-1} are shown in Fig. 5. The absorption bands are tabulated in Table 2. The spectra indicate the presence of three absorption bands at 657, 545 and 372 cm^{-1} for the sample as prepared and the annealed sample at 600 °C. By increasing the annealing temperature ($T_a \geq 800$ °C), splitting in the absorption bands is observed. The first band at 675 cm^{-1} consists of the first primary absorption band υ_1^* and three shoulders $\nu_1(1)$, $\nu_1(2)$ and $\nu_1(3)$ at 670, 830 and 880 cm^{-1}, respectively; while the second band υ_2^* still without splitting. The third band at 385 cm^{-1} splits into two small bands ν_3 and ν_4 at 449 and 380 cm^{-1}, respectively. The band ν_3 could be attributed to

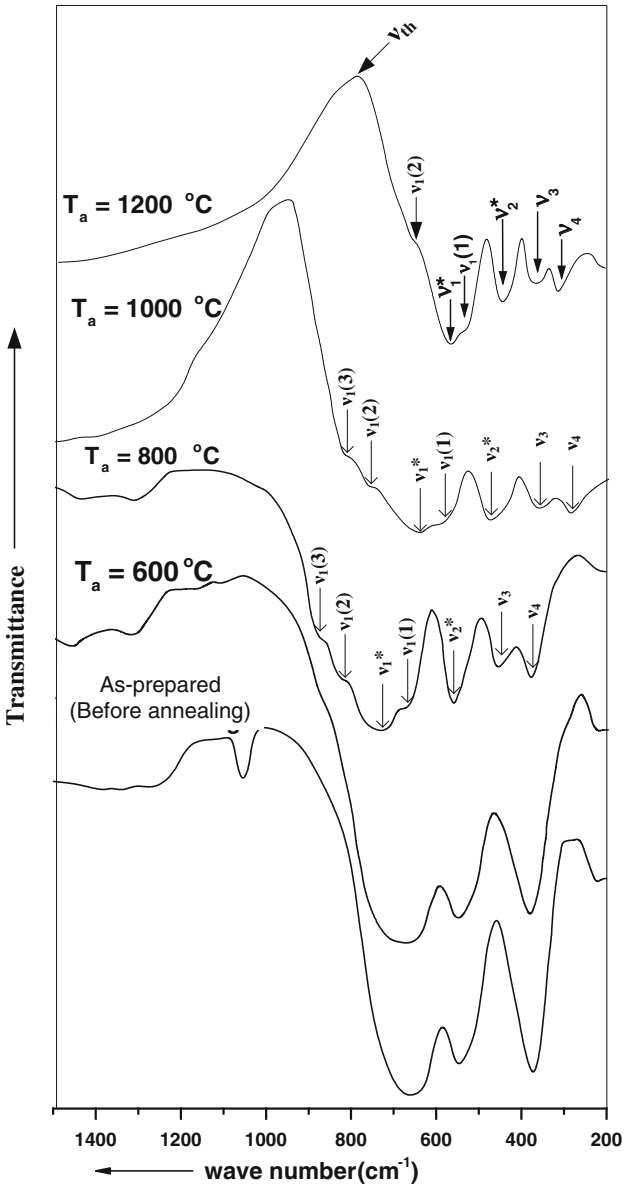

Fig. 5 IR absorption spectra for the lithium ferrite as prepared and annealed at 600, 800, 1,000 and 1,200 °C

Table 2 IR absorption bands of Li-ferrite

Annealing temperature (°C)	ν_1*	$\nu_1(1)$	$\nu_1(2)$	$\nu_1(3)$	ν_2*	ν_3	ν_4	ν_{th}	θ_D (K)
As prepared	657	–	–	–	545	372			
600	675	–	–	–	549	385	–	–	880
800	735	671	830	880	563	449	380	–	933
1,000	640	591	763	825	475	355	285	953	801
1,200	566	529	658	–	445	360	310	790	726

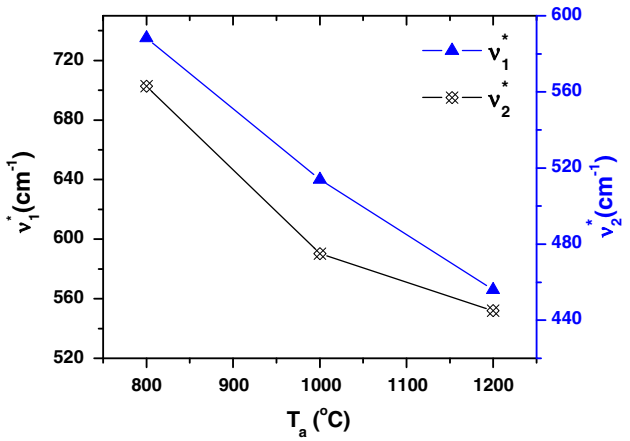

Fig. 6 The change in the frequency of the primary bands υ_1* and υ_2* with the annealing temperature

divalent metal ion–oxygen complexes in octahedral sites. Hence, its appearance gives an indication to the presence of a small amount of Fe^{2+} ions in the above-mentioned samples (Mazen et al. 1997). The fourth vibrational band υ_4 (around 265 cm^{-1}) is due to the lattice vibration (Josylu and Sobhanadri 1981). It has been shown by Potakova et al. (1972) that the presence of Fe^{2+} ions in ferrites can produce splitting or shoulder of absorption bands. It is attributed to Jahn–Teller distortion produced by Fe^{2+} ions which locally produce deformation in the crystal field potential and hence to the splitting of the absorption bands.

The spectra show change and shift in absorption bands by increasing the annealing temperature ($T_a \geq 800$ °C). For the tetrahedral site (A-site), the primary band υ_1^* shifted to lower frequency. Also, the two shoulders $\nu_1(1)$ and $\nu_1(2)$ are shifted to lower frequency at 529 and 658 cm^{-1}, respectively; while the third shoulder $\nu_1(3)$ disappeared completely at 1,200 °C. For the octahedral site (B-site), the band υ_2^* shifted to lower frequency; the two bands ν_3 and ν_4 shifted to lower values of wave number at 355 and 380 cm^{-1} (for $T_a = 1{,}000$ °C) and shifted to higher frequencies at $T_a = 1{,}200$ °C.

Figure 6 shows the behaviour of the primary bands of the tetrahedral site υ_1^* and the octahedral site υ_2^* with increasing the annealing temperature (from 800 up to 1,200 °C). It is obvious that the two bands υ_1^* and υ_2^* shifts towards the lower frequency. Also a difference in the band position of υ_1^* (in the range 735–566 cm^{-1}) and υ_2^* (in the range 563–445 cm^{-1}) is expected because of the difference in Fe^{3+}–O^{2-} distance for the tetrahedral and octahedral complexes. It was found that the Fe–O distance of the A-site (0.189 nm) is smaller than that of the B-site (0.199 nm) (Evans and Hafner 1968).

According to Waldron (1955), the threshold frequency for the electronic transition can be determined from the maximum point of the absorption spectra at which it reaches a limiting value. Figure 5 shows these threshold values for $T_a = 1{,}000$ and 1,200 °C, only and the estimated values are tabulated in Table 2. Also, the Debye temperature can be calculated using the following relation (Waldron 1955):

$$\theta_D = \frac{\hbar C v_{av}}{k} \tag{7}$$

where, $v_{av} = \frac{v_A + v_B}{2}$, v_A is the frequency of the primary band of A-site, v_B is the frequency of the primary band of B-site, $\hbar = h/2\pi$, h is the Plank constant, k is the Boltzmann's constant and $C = 3 \times 10^{10}$ cm/s; is the velocity of light. The calculated values of the Debye temperature are tabulated in Table 2. It can be noticed that the values of the Debye temperature decrease with increasing the annealing temperature from 933 to 726 K for $T_a = 800$ °C up to 1,200 °C, respectively.

Magnetic properties

Magnetic measurements of lithium ferrite annealed at 600, 800, 1,000 and 1,200 °C were performed using the vibration sample magnetometer (VSM) technique and the results of magnetic hysteresis at room temperature (300 K) and shown in Fig. 7. The saturation magnetization (M_s) and coercivity (H_C) were determined from the hysteresis graphs and listed in Table 3. It is known that the shape and the width of the hysteresis loop of a ferrite depend not only on the chemical composition, which determines the intrinsic properties, but also various factors connected with the sintering process such as porosity and grain size (Cullity 1959). From Fig. 7, it is observed that the relative area of all samples is small and the loop is thin and narrow which is a specific criterion for soft ferrite (Cullity 1959). Moreover, it can be noticed that the annealing temperature has a pronounced effect on the area of the hysteresis loop.

Figure 8 shows the variation of saturation magnetization (M_s) as a function of annealing temperature, where the saturation magnetization values are estimated from the highest value of M. The saturation magnetization increases with increasing the annealing temperature from 600 to 800 °C by 72 % then slightly increases by 11 % from 800

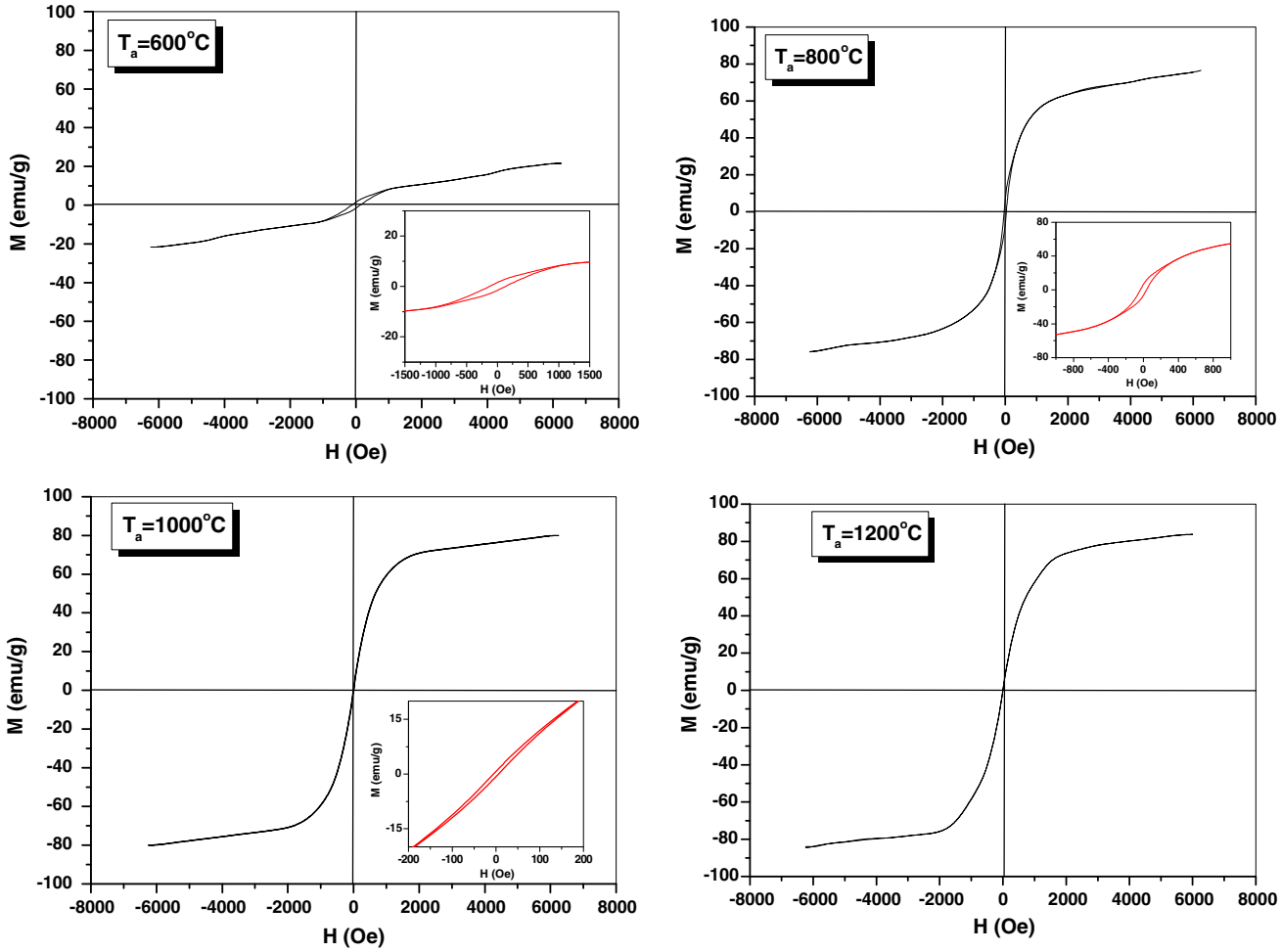

Fig. 7 Hysteresis curve for $Li_{0.5}Fe_{2.5}O_4$ powder annealed at 600 and 800 °C

Table 3 Magnetic parameters (Ms and H_C) and the activation energy from dc conductivity for lithium ferrite annealed at different temperatures

T_a (°C)	M_s (emu/g)	H_C (Oe)	E_σ (eV)
600	21.67	124.14	–
800	76.55	38.12	0.83
1,000	79.56	8.41	0.86
1,200	84.86	2.25	0.72

to 1,200 °C. The rather low value of M_s (21.67 emu/g) for the annealed sample at 600 °C may be due to the small particle size, existence of the remaining initial oxides and high density of structural defects. The highest saturation magnetization is (84.86 emu/g) for the annealed powder at 1,200 °C. The increase in saturation magnetization with increasing the annealing temperature may be due to pure phase formation of lithium ferrite and the reduction of defects in the annealed powders. Similar results have been reported in literature for Li- ferrite prepared by sol–gel auto-ignition method (Shirsath et al. 2011).

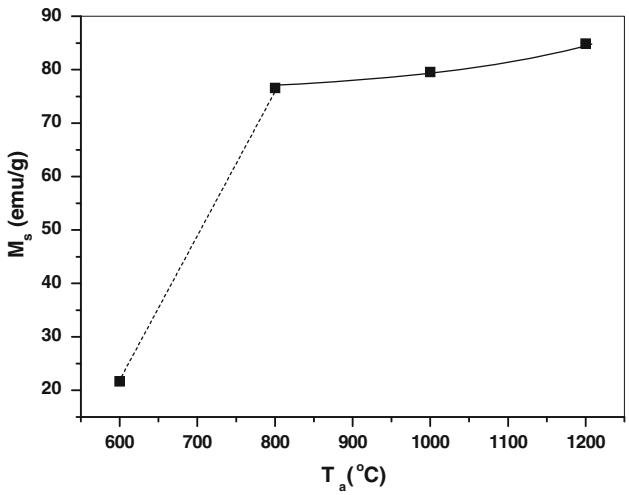

Fig. 8 The influence of annealing temperature on saturation magnetization

Figure 9 shows the coercivity (H_C) as a function of annealing temperature. The lowest value ($H_C = 2.25$ Oe) was recorded for the annealed powder at 1,200 °C. It is

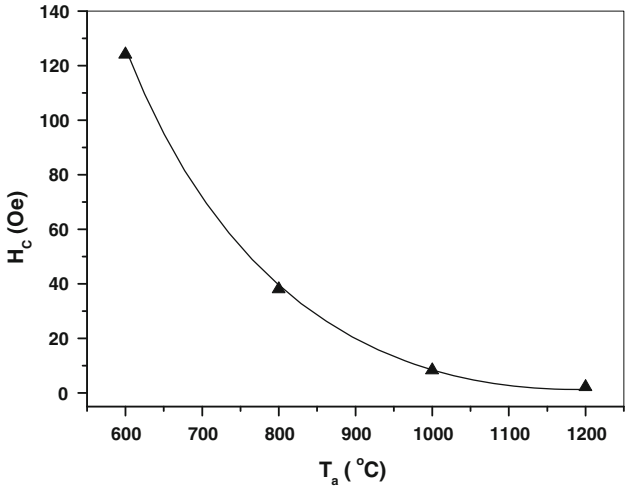

Fig. 9 The variation of coercivity with annealing temperature

noticed that the coercivity decreases with increasing the annealing temperature, which can be explained as follows: Above 600 °C, the particle size increases, thereby decreasing the number of grain boundaries, decreasing the structural defects and subsequently decreased the values of coercivity (Waje 2010).

Electrical properties

Effect of temperature on dc and ac electrical conductivity

The variation of dc and ac electrical conductivity with temperature has been studied for the annealed samples at 800, 1,000 and 1,200 °C. The measurements were carried out over a wide range of temperature from 300 to 750 K; the ac electrical conductivity was measured in the range of frequencies from 10^2 to 10^6 Hz. The logarithm of conductivity (ln σ) as a function of reciprocal temperature (T^{-1}) is shown in Fig. 10. The behaviour of lnσ versus T^{-1} could be divided into two regions (I and II). Region I lies below 650 K for the annealed sample at 800 °C, meanwhile lies below 365 K for other samples. For the annealed sample at 800 °C, the conductivity remains approximately constant with increasing the temperature in region I. This behaviour seems as an insulator behaviour may be attributed to the effect of nanoparticle size and as all the most of the oxides. The nanoparticle size means an increase in the number of grain boundaries, which acts as an insulator, and more thermal energy is required for electron exchange between Fe^{2+} and Fe^{3+} ions. But by increasing the annealing temperature, the particle sizes increase and the number of grain boundaries decreases. So the insulator behaviour disappears with increasing T_a above 800 °C and region II becomes as semiconductor behaviour. In the second region II, the conductivity increases with increasing temperature continuously. Accordingly, the lithium ferrite shows a semiconducting trend in this region, which is commonly seen in most ferrites and can be represented by Arrhenius relationship:

$$\sigma = \sigma_o \exp\left(\frac{-E_\sigma}{KT}\right) \tag{8}$$

where σ is the specific conductivity, σ_o is constant weakly temperature dependent, E_σ is activation energy, K is Boltzmann constant and T is the absolute temperature. The values of the activation energy have been calculated for the dc conductivity in region (II). The calculated values are tabulated in Table 3. It can be noticed that, the activation energy for the annealed samples at 800, 1,000 and 1,200 °C is 0.83, 0.86 and 0.71 eV, respectively. The values of the activation energy are due to a formation of small polaron (Kliger 1977).

Effect of frequency at room temperature

The ac conductivity as a function of frequency ($f = 10^2$–10^6 Hz) at room temperature for the annealed samples at 800, 1,000 and 1,200 °C is shown in Fig. 11. It is evident from the figure that the conductivity remains almost constant in the low frequency region but exhibits dispersion for higher frequencies ($f > 10^4$ Hz). The dispersion in $\tilde{\sigma}$ with frequency has been explained by Koops (1951) theorem, which supposed that the ferrite compact composed of two layers: grain with high conductivity and grain boundary with poor conductivity. At lower frequencies, grain boundaries are effective with high resistance giving a constant conductivity. At higher frequencies, the increase in conductivity is due to grain effect and also due to increase in hopping of charge carriers Fe^2–Fe^{3+} at the adjacent octahedral sites.

The effect of annealing temperature on the conductivity is shown in Fig. 11, where the conductivity increases with increasing the annealing temperature. This behaviour can be related to the presence of a higher number of Fe^{2+} formed at elevated annealing temperatures. As a result the probability for hopping between $Fe^{2+} \leftrightarrow Fe^{3+}$ increases, so the conductivity increases with T_a. Also the increase in conductivity may be related to the decrease in porosity with the annealing temperature since pores are non-conductive and the charge carrier face the pores during the hopping.

Figure 12 shows the variation of dielectric constant (ε') as a function of frequency for the annealed samples at (800, 1,000 and 1,200 °C). It is observed that, the dielectric constant (ε') decreases with increasing the frequency. This observed behaviour could be explained by Koops (1951) phenomenological theory. In this model, the dielectric structure of ferrites was supposed to be made of well-conducting layer of grains followed by poorly conducting

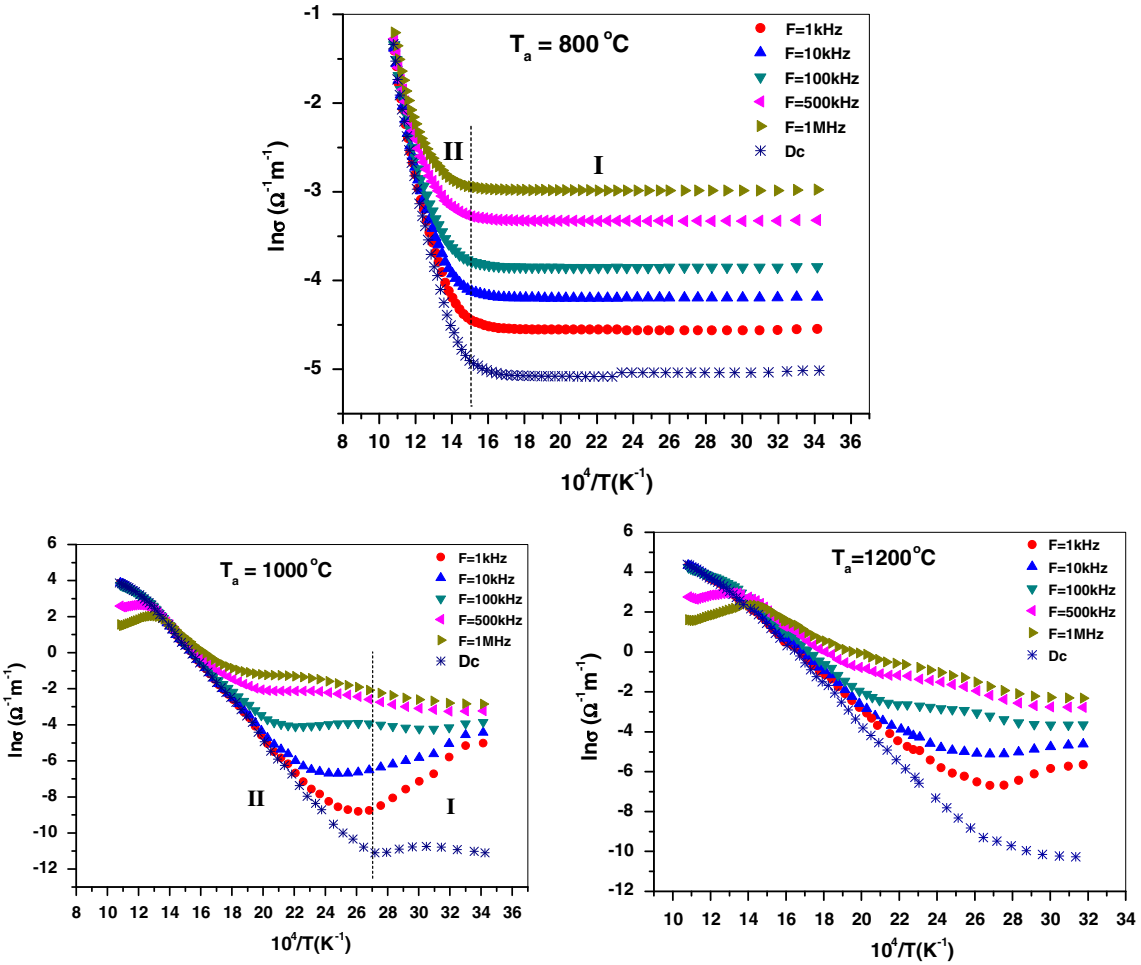

Fig. 10 Temperature dependence of ac and dc conductivity at various frequencies for *T*a = 800, 1,000 and 1,200 °C

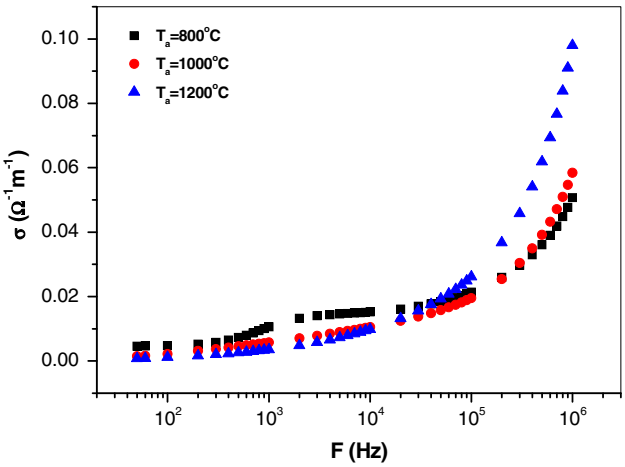

Fig. 11 Plot of σ versus frequency at room temperature for *T*a = 800, 1,000 and 1,200 °C

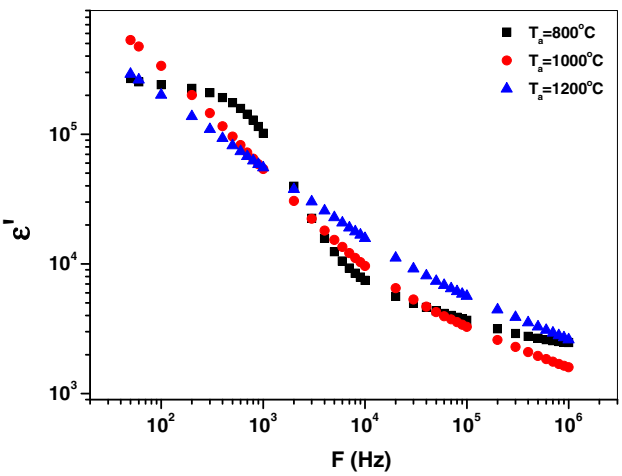

Fig. 12 Plot of ε' versus frequency at room temperature for *T*a = 800, 1,000 and 1,200 °C

layer of grain boundaries. Under the influence of electric field, the motion of charges in grains is interrupted at grain boundaries. This causes localized charge accumulation at the interface, which results in interfacial polarization. The decrease of polarization with increasing frequency may be due to the fact that beyond a certain frequency of the

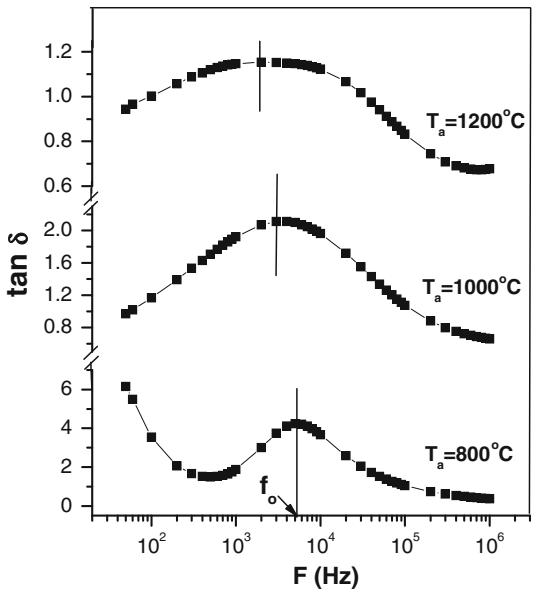

Fig. 13 Plot of tanδ versus frequency at room temperature for $Ta = 800$, 1,000 and 1,200 °C

electric field, the electronic exchange between Fe^{2+} and Fe^{3+} cannot follow the alternating field, hence the real part of dielectric constant (ε') decreases with increasing frequency.

The variation of loss tangent (tan δ) with frequency has been studied as shown in Fig. 13 for the annealed samples at 800, 1,000, 1,200 °C, respectively. Dielectric loss arises when the polarization lag behind the applied alternating field which is caused by the impurities and imperfections in the crystal. Anomalous or abnormal dielectric behaviour (relaxation peaks) are observed for all samples at ($f = f_o$). This peaking behaviour is explained by Rezlescu model (Rezlescu and Rezlescu 1974). According to this model, the peaking behaviour is obtained when the frequency of charge hopping between the Fe^{2+} and Fe^{3+} exactly matches with the frequency of the external applied field. The condition for maxima in the dielectric losses of a dielectric material is given by the relation:

$$\omega_o \tau = 1 \quad (8)$$

where $\omega_o = 2\pi f_o$ and τ is the relaxation time. The relaxation time is related to the jumping (hopping) probability per unit time, p, by the equation

$$\tau = 1/2p \text{ or } f_o \propto p. \quad (9)$$

Therefore, from the above relation it is clear that, maxima is observed when the jumping or hoping frequency of electrons between Fe^{2+} and Fe^{3+} becomes approximately equal to the frequency of the applied field. It is also evident from Fig. 13 that the value of (f_o) shifts to lower frequency with increasing the annealing temperature. Moreover, the relaxation time is calculated and found to be slightly increased with increasing the annealing temperature. The obtained values are $\tau = 3.18 \times 10^{-5}$, 4.55×10^{-5} and 7.96×10^{-5} s for $T_a = 800$, 1,000 and 1,200 °C, respectively.

Conclusions

1. $Li_{0.5}Fe_{2.5}O_4$ nanoparticles in the range of 26–70 nm were successfully synthesized using the milling process.
2. XRD patterns revealed the presence of some hematite phase for the annealed sample at 600 °C then by increasing the annealing temperature the samples were formed in single-phase cubic spinel structure.
3. IR spectra confirmed the formation of spinel structure and gave information about the distribution of ions between the two sites, tetrahedral (A-site) and octahedral (B-site).
4. The annealed sample at (1,200 °C) has the highest saturation magnetization (8 5 emu/g) and the lowest coercivity field (2.25 Oe).
5. The conductivity changed from insulator to semiconductor behaviour with increasing the annealing temperature.
6. The dielectric constant (ε') and loss tangent (tan δ) depend on the annealing temperature especially at high frequency.

References

Akther Hossain AKM, Mahmud ST, Seki M, Kawai T, Tabata H (2007) J Magn Magn Mater 312:210–219
Bahgat M, Farghaly FE, Abdel Basir SM, Fouad OA (2007) J Mater Process Technol 183:117
Bellad SS, Watawe SC, Chougule BK (1999) J Magn Magn Mater 195:57
Cullity BD (1959) Elements of X-ray diffraction. Addison-Wesley Publ., Boston
Evans BJ, Hafner S (1968) J Phys Chem Solids 29:1573
Hafner ST (1961) Z Kristallogr 115:331
Hashim M et al (2012) J Alloys Compd 518:11–18
Hessien MM (2008) J Magn Magn Mater 320:2800–2807
Josylu OS, Sobhanadri J (1981) Physica Status Solidi (a) 65:479
Kliger MI (1977) Phys Status Solidi B 79:9
Koops CG (1951) Phys Rev 83:121
Mazen SA, Metawe F, Mansour SF (1997) J Phys D Appl Phys 30:1799
Potakova VA, Zverv ND, Romanov VP (1972) Phys Stat Sol (a) 12:623
Rezlescu N, Rezlescu E (1974) Phys Status Solidi A 23:575

Shirsath SE et al (2011) J Magn Magn Mater 323:3104–3108
Smit J, Wijn HP (1959) Ferrites. Wiley, New York
Standley KJ (1972) Oxide magnetic materials. Clarendon press, Oxford
Tzeng Lue J (2007) In: Nalwa HS (ed) Encyclopedia of Nanoscience and Nanotechnology, vol 10. American Scientific Publishers, p 1
Verma V, Pandey V, Singh S, Aloysius RP, Annapoorni S, Kotanala RK (2009) Phys B 404:2309–2314
Waje SB, Hashim M, Daud W, Yusoff W, Abbas Z (2010) J Magn Magn Mater 322:686–691
Waldron RD (1955) Phys Rev 99:1727